Supplement of Atmos. Meas. Tech., 16, 247–271, 2023
https://doi.org/10.5194/amt-16-247-2023-supplement

Atmospheric Measurement Techniques
Open Access
EGU

Supplement of

Airborne flux measurements of ammonia over the southern Great Plains using chemical ionization mass spectrometry

Siegfried Schobesberger et al.

Correspondence to: Siegfried Schobesberger (siegfried.schobesberger@uef.fi)

Table of Contents

Further details on calibration experiments

Estimation of lab air humidity

Some of the follow-up calibration experiments at the University of Washington (UW) laboratories, denoted as set (2) in the main text, used dilution of dry N_2 with lab air (Fig. S2a, and orange circle in Fig. 2). We estimated the relative humidity (RH) of that lab air as 40 (±4) %, based on the temperature of 18 °C and dew point of 7 °C reported at nearby Boeing Field (airport KBFI) at the time, resulting in an RH range from 20% to 36% for the corresponding measurements.

Increased sensitivities following instrument startup

A noteworthy observation during the HI-SCALE deployment was made during sensitivity tests for organic compounds made in the field, before and after research flights. For those tests, a small flow (≤ 10 sccm) of calibrant-containing N_2 from a cylinder (1 ppmv of isoprene, 1 ppmv of α-pinene and 0.5 ppmv of dimethyl sulfide, ±5% each, in UHP N_2; Scott-Marrin) was mixed into a large flow of dry N_2 (> 25 L min^{-1}) that was directed into the CIMS inlet tip outside the aircraft, while the CIMS sample pump pulled 22 L min^{-1} towards the instrument. Invariably, significantly higher sensitivities were obtained before flights than after flights (Fig. S2b). The mechanism behind that remained unresolved, and the only co-varying circumstance was found to be the relative abundance of dimer reagent ion counts, which we expressed as the monomer-to-dimer ratio $[C_6D_6^+]/[C_6D_6.C_6D_6^+]$. We speculate that the benzene mixing ratios in the IMR could have been higher pre-flight, which also coincided with the first 1-2 hours after instrument start-up, and responsible for those observations. We could not exclude that these observations are only seen when using dry N_2, as attempts of mixing calibration gas with ambient air produced inconclusive results for those organics (example shown in Fig. S2c). The calibration experiments for NH_3 never occurred at times of low enough (< ~5) ratios $[C_6D_6^+]/[C_6D_6.C_6D_6^+]$, so we could not establish if the response of $NH_3.C_6D_6^+$ was subject to any dependence on that ratio (Fig. S2c).

Overall NH_3 levels observed during IOP1

An overview of all the mixing ratios obtained during 11 research flights (RF) in May 2016 is presented in Fig. S3. Below ~900 m AMSL (~600 m above the SGP site), the observed NH_3 mixing ratios broadly ranged from 1 to 10 ppbv, and up to 10s of ppbv in plumes. Observations above 900 m covered a larger number of flights and ranged down to 100 pptv, including the flight yielding data from the highest altitude (4200 m AMSL) as well as the lowest average mixing ratios. The observations at the lower end (100-400 pptv) occurred on May 16 (RF14) and 19 (RF16), which were dominated by clouds, and did not include measurements below cloud base. Mixing ratios then remained as low when climbing higher into the free troposphere. Observations of NH_3 mixing ratios of ~1 ppbv or higher are associated with overall sunny days and were made clear of cloud and with good confidence also within the well-mixed boundary layer.

WRF-Chem model configurations

We used the community regional Weather Research and Forecasting Model coupled to chemistry (WRF-Chem version 4.2) for generating modeling results in this study. Specifically, WRF-Chem was run for the times of RF13, i.e., the afternoon of 14 May 2016. Resulting NH_3 mixing ratios for the full domain are shown in Fig. S10. Figure 6 includes the results for the model cells crossed by the aircraft during RF13.

Our configuration of the WRF-Chem model included a domain covering most of the Midwest, Eastern and Southern parts of the United States at a grid spacing of 12 km. Gas-phase chemistry represented by the SAPRC-99 mechanism was coupled with the MOSAIC (Model for Simulating Aerosol Interaction and Chemistry) aerosol module (Zaveri et al., 2008) and includes aerosol chemistry and secondary organic aerosol updates as described in Shrivastava et al. (2022). We used the NEI 2017 emissions inventory for anthropogenic emissions in the USA, while biomass burning emissions were from the 2014 Quick Fire Emissions Database (QFED v2.5) inventory and were coupled to the Freitas plume rise model (Freitas et al., 2007). WRF-Chem used online biogenic emissions calculated using the Model of Emissions of Gases and Aerosols from Nature (MEGAN v2.1; Guenther et al., 2012) coupled within the land surface scheme of Community Land Model version 4 (CLM4) in WRF-Chem version 4.2. We have recently implemented within WRF-Chem a mechanistic soil NO_x emission scheme based on that of Rasool et al. (2019), along with NH_3 emissions derived from Dubache et al. (2019). The total NH_3 emissions fluxes simulated in WRF-Chem are a sum of those from NEI 2017 (Fig. S11) and the soil NH_3 emissions (Fig. S12) that we recently implemented.

Additional details are provided in Table S1.

Table S1: WRF-Chem model configurations used in this work

WRF domain	12 km horizontal grid resolution with 45 vertical layers
Planetary Boundary layer (PBL)	Yonsei University (YSU) PBL scheme (Hong, 2010)
Land Surface Model	Community Land Model (CLM v4) (Lawrence et al., 2011)
Cloud microphysics	Morrison double moments (Morrison et al., 2009)
Radiation	RRTMG scheme (longwave + shortwave) (Iacono et al., 2008)
Convective parametrization	Grell and Freitas (2014). Grid-scale wet removal: Easter et al. (2004)
Aerosol-Cloud interactions	Aerosol activation based on the parameterization by Abdul-Razzak and Ghan (2002)
Emissions	NEI 2017 for anthropogenic aerosol and trace gas emissions, QFED v2.5 for biomass burning emissions, biogenic emissions from MEGAN2.1 (Guenther et al., 2012)
Gas-phase photochemistry	SAPRC-99
Aerosol chemistry	MOSAIC for inorganic aerosols, secondary organic aerosol treatments as described in Shrivastava et al. (2022)
Boundary conditions	0.25-degree GFS final analysis (FNL) for meteorology and CAM-Chem global model simulations for aerosols and trace gases

Wavelet power spectra for temperature measurements

Figure S7 includes power spectra for ambient temperature (T) measured by either the AIMMS or the Rosemount sensor. Turbulence was captured well by the w measurements up to highest frequencies, whereas the Rosemount's 1-Hz T measurements were somewhat attenuated at frequencies > 0.3 Hz. Interestingly, the power spectra for the AIMMS T measurements, nominally at 20 Hz, did not reveal any attenuation, even though visual comparisons of the two T time series suggested that the Rosemount sensor reacted considerably faster to T changes. Also, sensible heat flux calculations, prepared for a separate publication, produced more reasonable results when using the Rosemount data. The high spectral power of the AIMMS T measurements beyond ~0.3 Hz may instead be due to instrument noise.

Figures S1-S12

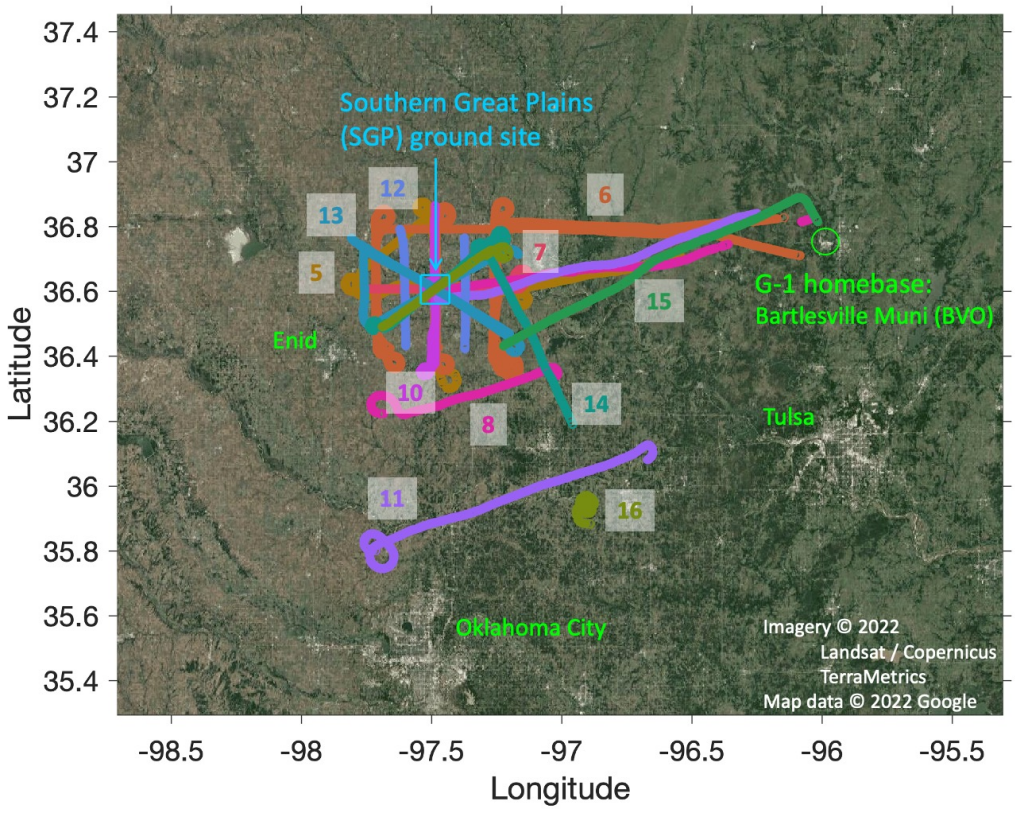

Fig. S1: Portions of flight tracks of the research flights 5-8 and 10-16 when operating in benzene-CI (positive polarity) mode. These flights took place during the intensive operating period of HI-SCALE in spring 2016 (IOP1), specifically May 2, 3, 6, 7, 10, 11, 13, 14, 16, 18 and 19, respectively. Each flight has the same separate color as used in the vertical NH_3 mixing ratio profiles shown in Fig. S3.

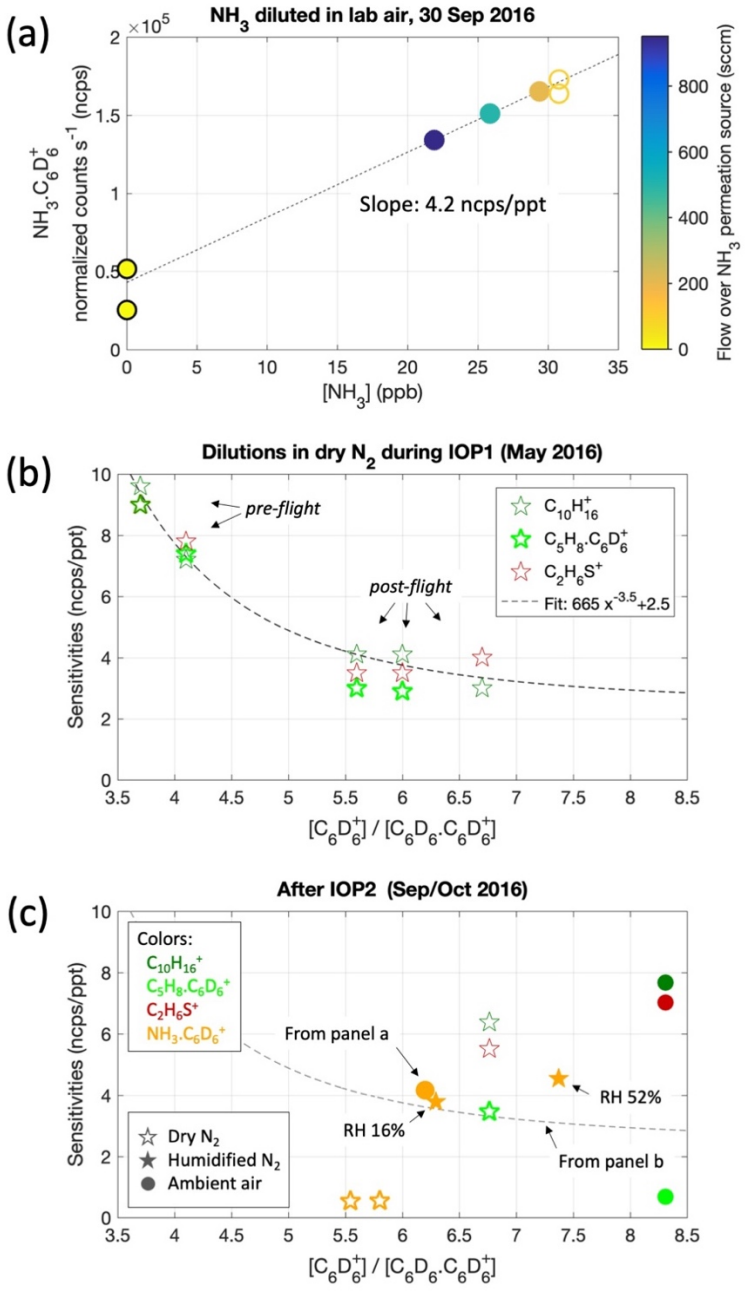

Fig. S2: Results of various calibration experiments. **(a)** Response of normalized $NH_3.C_6D_6^+$ count rate to NH_3 mixing ratios obtained from diluting a permeation device output with room air, yielding a sensitivity of 4.2 ncps/pptv. Results with permeation source flows < 150 sccm (open circles) produced less reproducible results. Background counts (black-rimmed yellow) are from both before (lower counts) and after delivering NH_3. **(b)** Sensitivities obtained for isoprene (C_5H_8, light green), α-pinene ($C_{10}H_{16}$, dark green) and dimethyl sulfide (C_2H_6S, red) in dry N_2 during calibration experiments in the field, as a function of the ratio of reagent ion mono- and dimer count rates. **(c)** Various sensitivity calibration results obtained shortly after HI-SCALE, including results in ambient (i.e., humid) air (circles) and for NH_3 (orange).

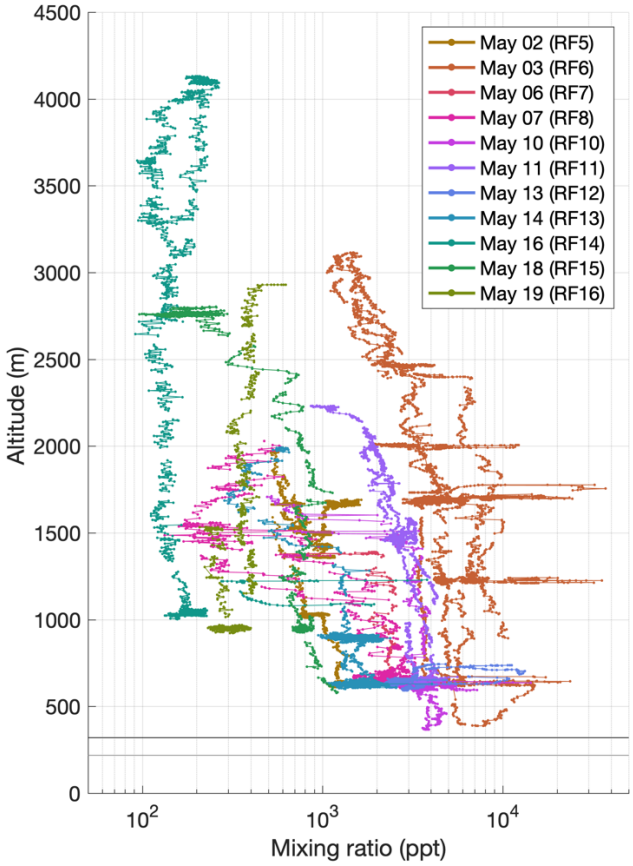

Fig. S3: Overview of NH_3 mixing ratios (pptv) retrieved during 11 flights (research flights 5-8 and 10-16) in May 2016, as a function of altitude (m above mean sea level). These are all results obtained from CIMS in standard benzene-CI mode during IOP1 of HI-SCALE. Each color corresponds to a separate flight, using the same color coding as in Fig. S1.

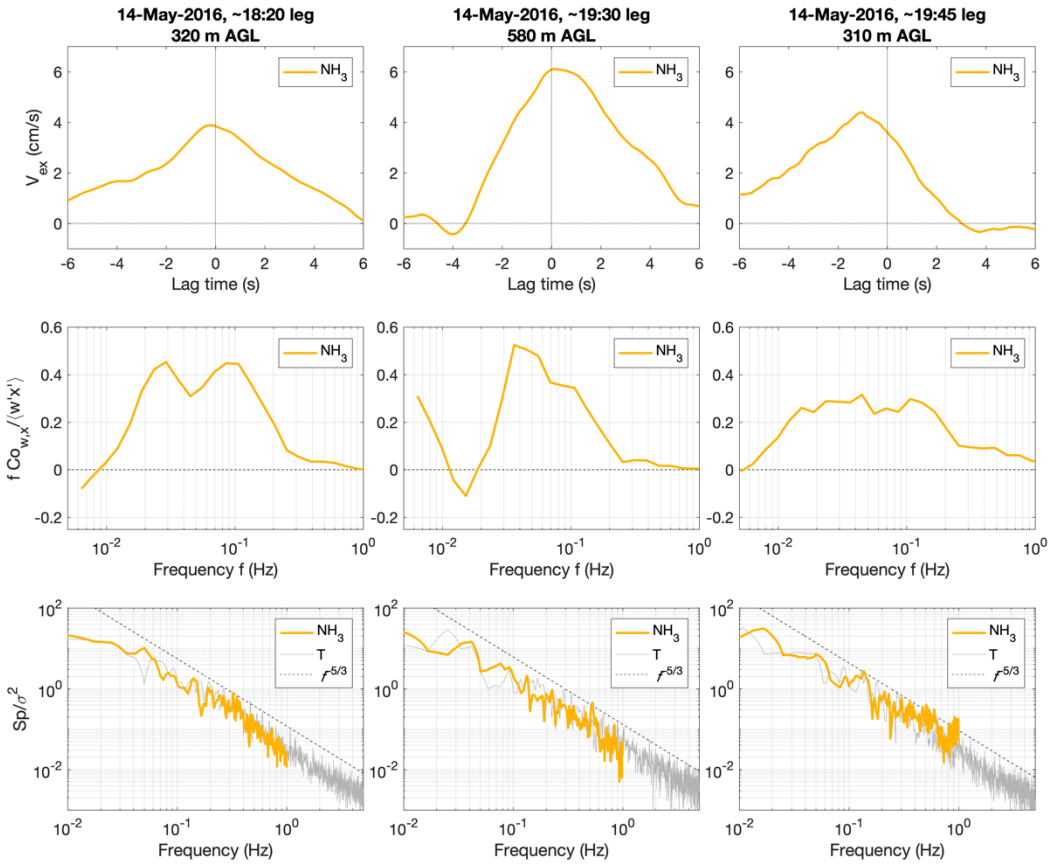

Fig. S4: Metrics of eddy-covariance analysis using the ensemble-average method for the three legs in Fig. 6. Shown, for each leg, are averages of all 2-min time intervals (blue in Fig. 6) that fulfill the quality criteria, in particular including stationarity, a total of 11 periods. The top row shows normalized covariance (i.e., exchange velocity, V_{ex}) as a function of time lag. Covariance maximized close to zero delay relative to the wind data (–0.01 ± 0.74 s); consequently, zero lag was used for this flight. The likely main cause of lag was drifts in data acquisition clocks. Times were synchronized (±0.003 s or better) pre-flight, but net drifts of up to ±0.1 s per hour were commonly found post-flight. The center row shows frequency-weighted and flux-normalized co-spectra for x = [NH_3] and w. The bottom row presents variance-normalized power spectra for [NH_3] and temperature, exhibiting the –5/3 decay expected for the inertial subrange (dashed line) and indicating negligible high-frequency attenuation.

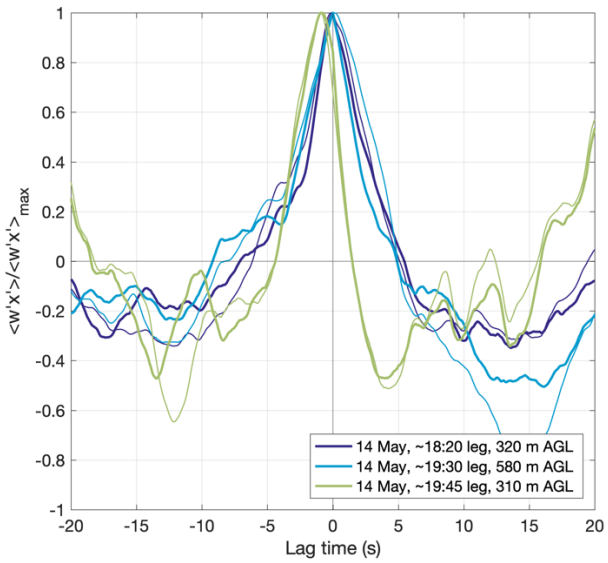

Fig. S5: Covariance of vertical wind (w) and NH_3 mixing ratio (x) as a function of lag time for the three legs in Figs. 6-7; calculated by fast Fourier transform (thin lines) and wavelet coefficients (thick lines).

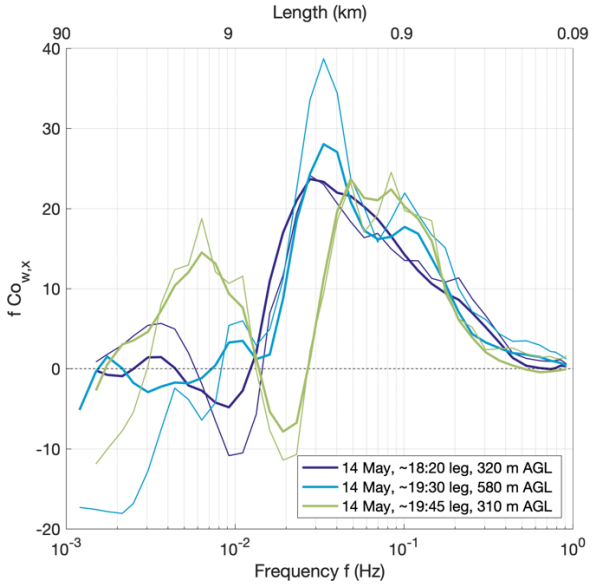

Fig. S6: Frequency-weighted co-spectra for x = [NH_3] and w for the three legs in Figs. 6-7, calculated by time-averaging the CWT co-spectra (thick lines) and by fast Fourier transform of the same period (thin lines).

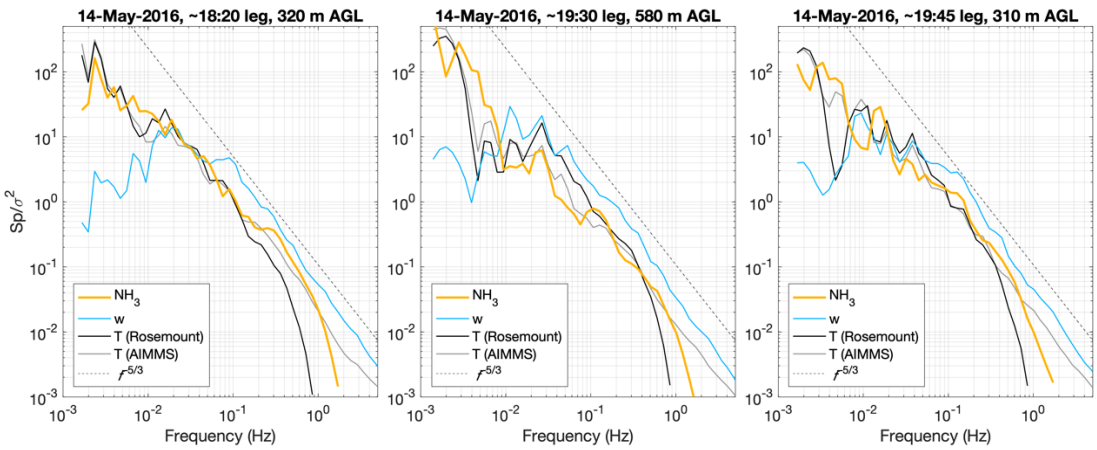

Fig. S7: Variance-normalized CWT power spectra for the three legs in Figs. 6-7, exhibiting the –5/3 decay expected for the inertial subrange (dashed line) and indicating negligible high-frequency attenuation, at least up the Nyquist frequencies (1 Hz for NH_3, 0.5 Hz for Rosemount, 5 Hz for AIMMS), analogously to the power spectra in Fig. S4 (bottom row).

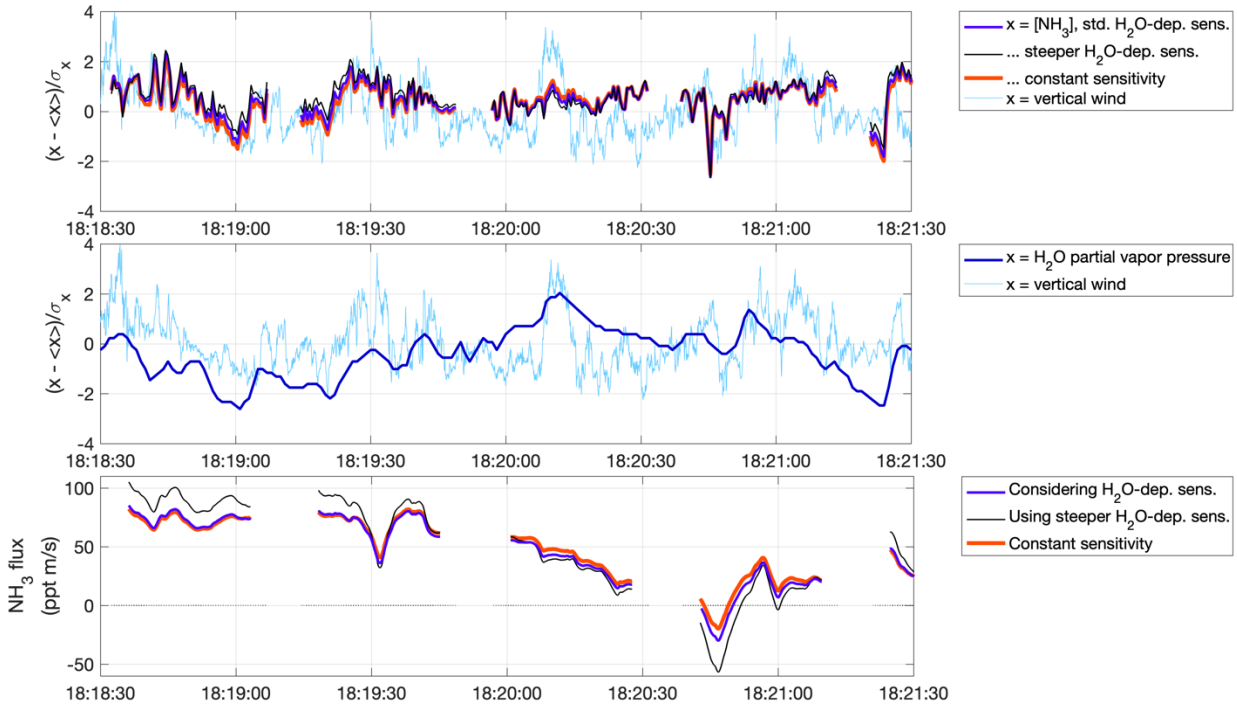

Fig. S8: Top and center panel: Fluctuations of vertical wind, water vapor and NH_3 mixing ratio measurements ([NH_3]) during part of the first case study leg during RF13 on 14 May (cf. Fig 7). The [NH_3] time series (top panel) are shown: as calculated for this study, i.e., accounting for humidity-dependent sensitivity (blue), as resulting without accounting for it (red), and as resulting if using a steeper humidity dependence (black; cf. Fig. 2). The water partial vapor pressure fluctuations (center panel) yielded a leg-wide flux of 0.078 ± 0.037 torr m s^{-1}. The bottom panel presents the resulting CWT fluxes obtained for NH_3 with (blue) and without (red) accounting for humidity-dependent sensitivity to NH_3, as well as when using the steeper humidity dependence (black).

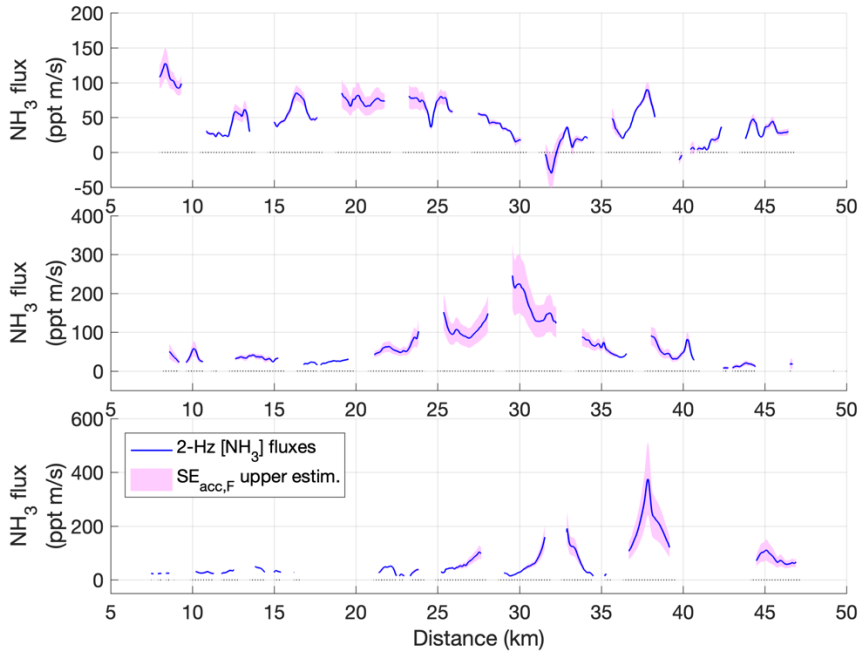

Fig. S9: 2-Hz CWT fluxes for the three straight-and-level legs of our case study (flight RF13). Magenta shades indicate our upper-end estimates for the systematic flux errors due to uncertainties in instrument sensitivity ($SE_{acc,F}$). The minimum uncertainty is ±5%. Larger $SE_{acc,F}$ are due to variability in ambient absolute humidity, combined with a conservative estimate of our understanding of the sensitivity's humidity dependence. A more detailed description is found in Sect. 3.8.

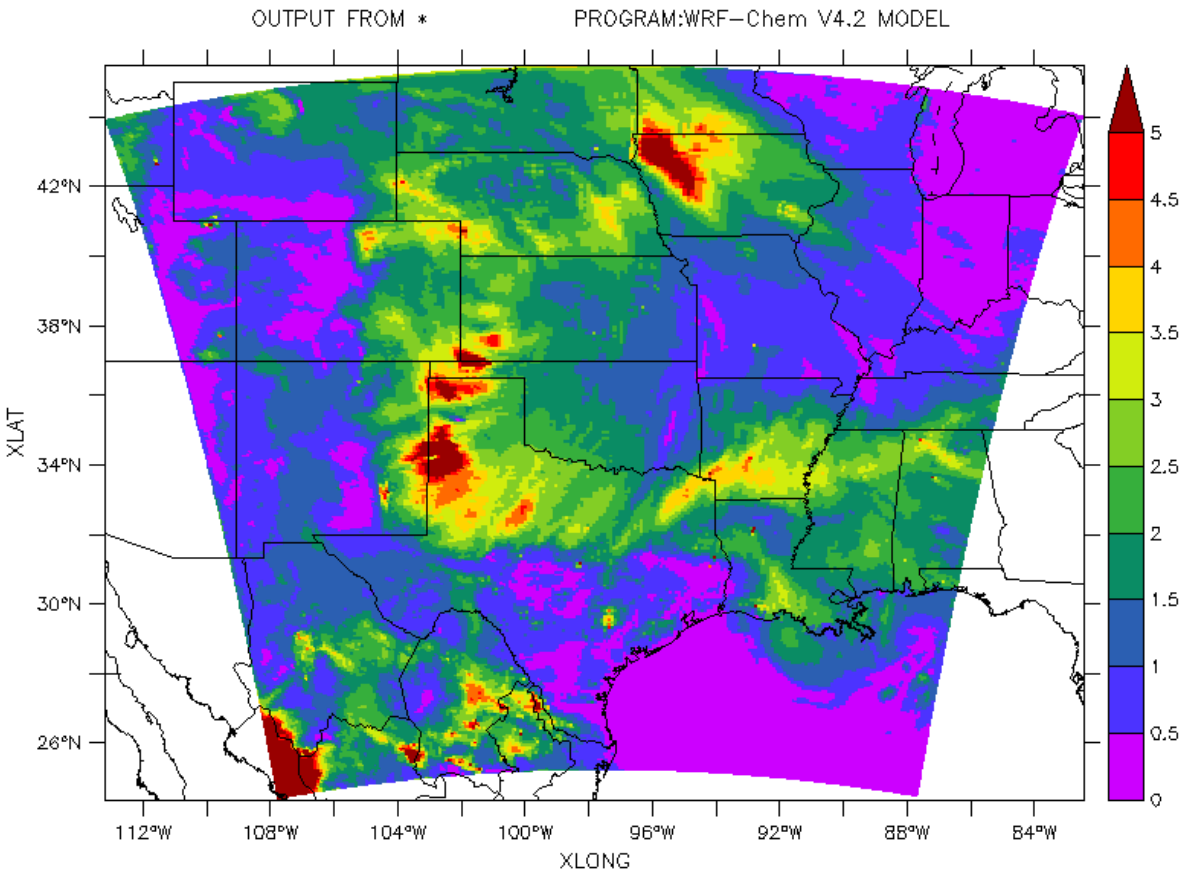

Fig. S10: NH_3 mixing ratios (color scale from 0 to 5 ppbv) resulting from WRF-Chem model simulations for 14 May 2016, 20:00 UTC, i.e., during RF13. The RF 13 flight tracks discussed in the main text (Fig. 6) were centered on the SGP ground site, located at the center of this map (36.61° N, 97.49° W).

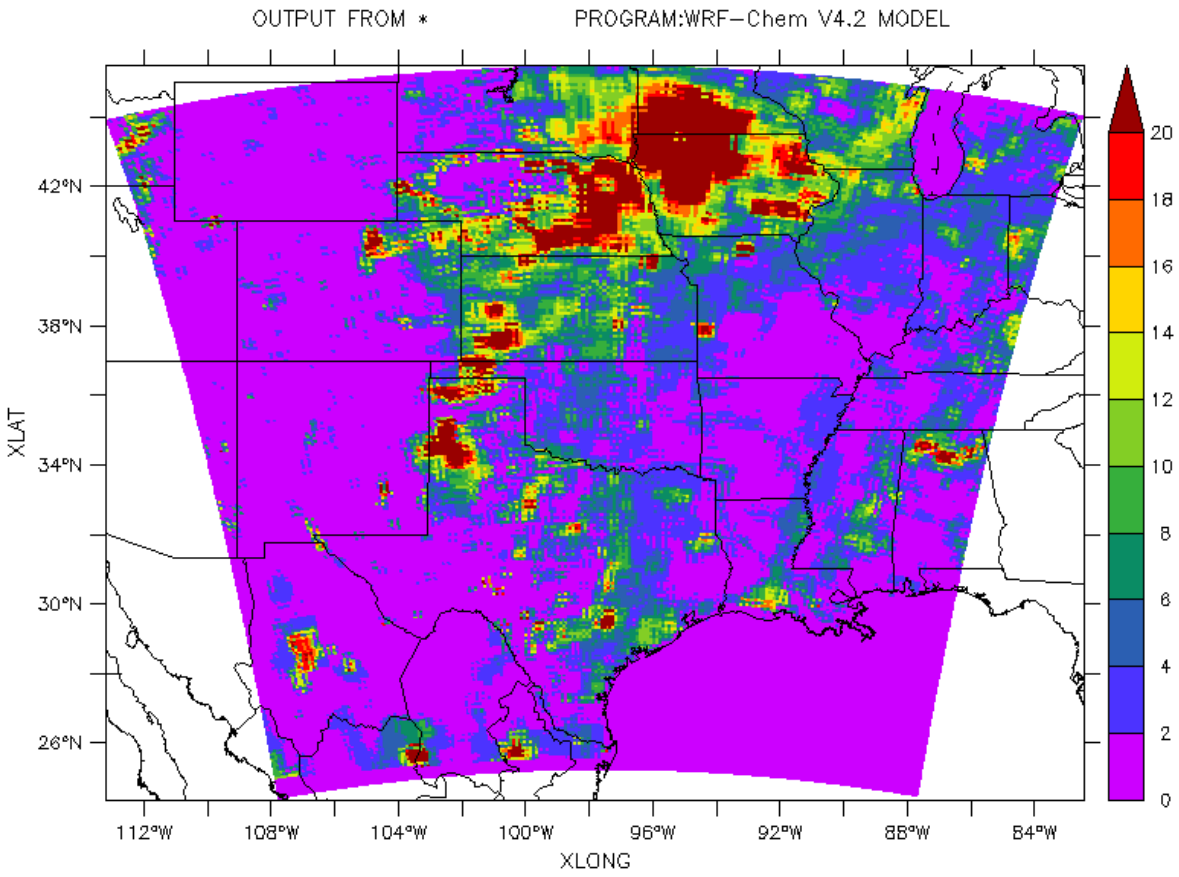

Fig. S11: Emissions of NH_3 in the National Emissions Inventory (NEI, 2017 data) for 14 May 2016 20:00 UTC. They do not include emissions from soils related to N cycling (Fig. S12), which we additionally included in the WRF-Chem model simulation. The color scale ranges from 0 to 20 mol km^{-2} h^{-1}. The map is centered on the SGP ground site at 36.61° N, 97.49° W.

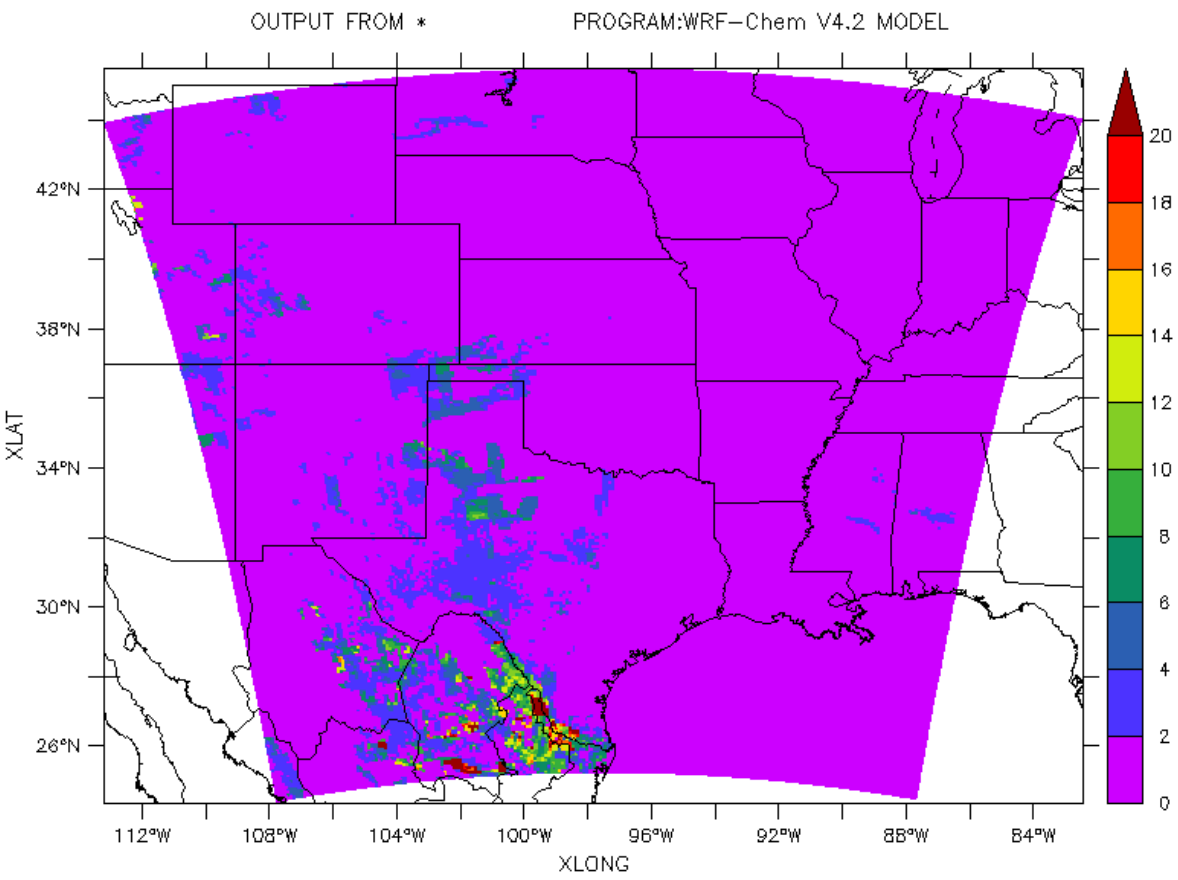

Fig. S12: Emissions of NH_3 in the mechanistic soil NO_x emission scheme that were added to the NEI emissions in WRF-Chem model simulation. The color scale ranges from 0 to 20 mol km^{-2} h^{-1}. The map is centered on the SGP ground site at 36.61° N, 97.49° W. For the area of RF13, and indeed of all flights of HI-SCALE IOP1, the scheme yielded additional NH_3 emissions below 2 mol km^{-2} h^{-1} (purple) for 14 May 2016.

References

Abdul-Razzak, H. and Ghan, S. J.: A parameterization of aerosol activation 3. Sectional representation, J. Geophys. Res. Atmos., 107, AAC 1-1-AAC 1-6, 2002.

Dubache, G., Li, S., Zheng, X., Zhang, W., and Deng, J.: Modeling ammonia volatilization following urea application to winter cereal fields in the United Kingdom by a revised biogeochemical model, Sci. Total Environ., 660, 1403-1418, 2019.

Easter, R. C., Ghan, S. J., Zhang, Y., Saylor, R. D., Chapman, E. G., Laulainen, N. S., Abdul-Razzak, H., Leung, L. R., Bian, X., and Zaveri, R. A.: MIRAGE: Model description and evaluation of aerosols and trace gases, J. Geophys. Res. Atmos., 109, 2004.

Freitas, S. R., Longo, K. M., Chatfield, R., Latham, D., Silva Dias, M. A. F., Andreae, M. O., Prins, E., Santos, J. C., Gielow, R., and Carvalho Jr, J. A.: Including the sub-grid scale plume rise of vegetation fires in low resolution atmospheric transport models, Atmos. Chem. Phys., 7, 3385-3398, 2007.

Grell, G. A. and Freitas, S. R.: A scale and aerosol aware stochastic convective parameterization for weather and air quality modeling, Atmos. Chem. Phys., 14, 5233-5250, 2014.

Guenther, A. B., Jiang, X., Heald, C. L., Sakulyanontvittaya, T., Duhl, T., Emmons, L. K., and Wang, X.: The Model of Emissions of Gases and Aerosols from Nature version 2.1 (MEGAN2.1): an extended and updated framework for modeling biogenic emissions, Geosci. Model Dev., 5, 1471-1492, 2012.

Hong, S.-Y.: A new stable boundary-layer mixing scheme and its impact on the simulated East Asian summer monsoon, Quart. J. R. Met. Soc., 136, 1481-1496, 2010.

Iacono, M. J., Delamere, J. S., Mlawer, E. J., Shephard, M. W., Clough, S. A., and Collins, W. D.: Radiative forcing by long-lived greenhouse gases: Calculations with the AER radiative transfer models, J. Geophys. Res. Atmos., 113, 2008.

Lawrence, D. M., Oleson, K. W., Flanner, M. G., Thornton, P. E., Swenson, S. C., Lawrence, P. J., Zeng, X., Yang, Z.-L., Levis, S., Sakaguchi, K., Bonan, G. B., and Slater, A. G.: Parameterization improvements and functional and structural advances in Version 4 of the Community Land Model, J. Adv. Model. Earth Syst., 3, 2011.

Morrison, H., Thompson, G., and Tatarskii, V.: Impact of Cloud Microphysics on the Development of Trailing Stratiform Precipitation in a Simulated Squall Line: Comparison of One- and Two-Moment Schemes, Mon. Weather Rev., 137, 991-1007, 2009.

Rasool, Q. Z., Bash, J. O., and Cohan, D. S.: Mechanistic representation of soil nitrogen emissions in the Community Multiscale Air Quality (CMAQ) model v 5.1, Geosci. Model Dev., 12, 849-878, 2019.

Shrivastava, M., Rasool, Q. Z., Zhao, B., Octaviani, M., Zaveri, R. A., Zelenyuk, A., Gaudet, B., Liu, Y., Shilling, J. E., Schneider, J., Schulz, C., Zöger, M., Martin, S. T., Ye, J., Guenther, A., Souza, R. F., Wendisch, M., and Pöschl, U.: Tight Coupling of Surface and In-Plant Biochemistry and Convection Governs Key Fine Particulate Components over the Amazon Rainforest, ACS Earth Space Chem., 6, 380-390, 2022.

Zaveri, R. A., Easter, R. C., Fast, J. D., and Peters, L. K.: Model for Simulating Aerosol Interactions and Chemistry (MOSAIC), J. Geophys. Res. Atmos., 113, 2008.